Article

HKUST-1 as a Positive Electrode Material for Supercapattery

Nur Hawa Nabilah Azman [1]**, Muhammad Mustaqhim Alias** [2] **and Yusran Sulaiman** [1,2,*]

1   Functional Nanotechnology Devices Laboratory, Institute of Nanoscience and Nanotechnology (ION2), Universiti Putra Malaysia, Serdang 43400, Selangor, Malaysia; hawa.nabilah@upm.edu.my
2   Department of Chemistry, Faculty of Science, Universiti Putra Malaysia (UPM), Serdang 43400, Selangor, Malaysia; 196896@upm.edu.my
*   Correspondence: yusran@upm.edu.my

Abstract: The copper-based metal-organic framework (HKUST-1) exhibits interesting properties, such as high porosity and large specific surface area, which are useful as electrode materials for supercapattery. Herein, the HKUST-1 was synthesized through a facile hydrothermal method and exhibited a typical octahedral structure with a specific surface area of 1015.02 m^2 g^{-1}, which was calculated using the Barrett–Joyner–Halenda (BJH) method. From the three-electrode analysis, the HKUST-1 demonstrated a specific capacity of 126.2 C g^{-1} in 1 M LiOH. The structural fingerprint of the HKUST-1 was confirmed with Fourier-transform infrared spectroscopy, Raman spectroscopy, and X-ray diffraction spectroscopy. A supercapattery device, i.e., the HKUST-1//N-doped graphene, revealed a maximum specific power of 300 W kg^{-1} and a specific energy of 2.61 W h kg^{-1} at 1 A g^{-1} with 57% capacitance retention during continuous charging–discharging, even after 10,000 cycles. The HKUST-1 also demonstrated a low charge transfer resistance and a low equivalent series resistance of 7.86 Ω and 0.87 Ω, respectively, verifying its good conductivity. The prominent supercapattery performance of the HKUST-1//N-doped graphene suggested that the HKUST-1 is a promising positive electrode for supercapattery.

Keywords: supercapattery; copper-based metal-organic framework; nitrogen-doped graphene; battery type; specific capacity; specific energy

1. Introduction

Global warming, climate change, the greenhouse effect, and the emission of carbon dioxide are among the environmental issues that have become highly controversial topics worldwide nowadays. Many countries have taken preventive measures in order to minimize the effect of fossil fuels, i.e., petrol, diesel, and charcoal consumption, on the environment and human health. Green technology and net-zero carbon emission campaigns are part of the effort to establish a low carbon footprint. Green technologies, for instance, hybrid electric cars, solar energy, smart buildings, and wastewater treatment, have been developed to address the environmental and health problems related to pollutants. Therefore, effective energy-storing devices are urgently needed to store these sustainable and renewable energies in order to be utilized by consumers. There are a lot of available energy storage devices in the market such as batteries, supercapacitors, hydrogen energy storage, and fuel cells. Among them, supercapacitors and batteries are the most widely used by consumers in their daily lives. However, the performance of supercapacitors and batteries as single devices is not sufficient to meet the energy needed, as the world's population and technology keep growing rapidly every year. Thus, many researchers have been considering integrating two devices into a single novel device that can have both merits of the combined devices.

Supercapatteries are new and novel emerging energy-storing devices that bridge the void between the electrochemical performances of supercapacitors and batteries. Supercapacitors accumulate charges via electrostatic interactions known as electrical double-layer

capacitors and redox reactions, i.e., pseudocapacitors or both, depending on the types of materials used as the electrode materials. The materials that are used for electrical double-layer capacitors are materials like carbonaceous materials such as graphene derivatives, carbon nanotubes, and carbon nanofibers. The large specific surface areas and good mechanical strength of carbonaceous materials allow them to possess long life cycles and high specific power with low specific energy. Batteries that utilize battery-type materials, for instance, metal-organic frameworks and metal oxides store charges via Faradaic redox reactions, exhibit high specific energy and low specific power and poor life cycles. Supercapatteries are a combination of supercapacitors and batteries. The negative electrodes of the supercapatteries are made up of capacitor-type materials and the positive electrodes are fabricated from battery-type materials that allow the supercapatteries to exhibit higher specific power, greater specific energy, and longer life cycles in comparison to batteries and supercapacitors.

Metal-organic frameworks are types of materials that are fabricated by assembling organic ligands with metal centers and are widely used in energy storage applications like batteries, supercapacitors, and supercapatteries. Metal-organic frameworks are always preferred due to their large specific surface area and highly porous structure, which permits easy transportation of electrolyte ions, allowing the metal-organic frameworks to demonstrate high specific energy and high specific capacity for supercapattery [1,2]. The Hong Kong University of Science and Technology (HKUST-1), also known as MOF-199, is a copper-based metal-organic framework in which the copper atoms are coordinated by oxygen from trimesic acid linkers and water molecules. The HKUST-1 is one of the widely used metal-organic frameworks due to its high specific surface area, large pore volume, and excellent thermal stability. One of the most intriguing metal-organic frameworks that is usually used as an electrode for supercapattery is nickel phosphate (VSB-5). A composite of VSB-5 and reduced graphene oxide (rGO) (VSB-5/rGO) displayed a uniform meso-microporous structure with a specific surface area of 247.8 $m^2 g^{-1}$ that helps to maximize the electroactive area for electrochemical reactions. The composite unveiled a high specific capacity (117.3 $mAh g^{-1}$) with high specific energy (80.5 $Wh kg^{-1}$) [3]. As a device, the activated carbon//VSB-5/reduced graphene oxide, exhibited a maximum specific capacity of 86.8 $mAh g^{-1}$, and was able to retain 88% capacity retention, even after 5000 cycles.

Iqbal et al. [2] reported a cobalt metal-organic framework-based composite, i.e., a cobalt metal-organic framework/polyaniline (cobalt metal-organic framework/PANI), that exhibits specific capacity, specific energy, and specific power of 104 $C g^{-1}$, 23.2 $W h kg^{-1}$ and 1600 $W kg^{-1}$, respectively. The composite coexists in a well-blended structure with a three-dimensional structure consisting of various morphology, i.e., squares, rods, and rectangles, which synergistically enhance the supercapattteries' performance of the composite. The cobalt metal-organic framework/PANI revealed an IV-type isotherm curve, revealing its mesoporous structure with a specific surface area of 156.59 $cm^2 g^{-1}$. Ramasubbu et al. [4] revealed that a composite of cobalt metal-organic framework and titanium oxide (TiO_2) prepared via the sol–gel method revealed a high specific capacity of 111.2 $C g^{-1}$ with 93% capacity retention, even after 5000 charge–discharge cycles. This excellent electrochemical performance is due to the impressive morphology of the composite in which the well-interconnected network structure of the TiO_2 increases the specific surface area (289 $m^2 g^{-1}$) and porosity (pore volume = 0.29 $cm^2 g^{-1}$ and pore diameter = 4.32 nm). However, the composite illustrated a low specific energy of 0.4 $Wh kg^{-1}$, which was mainly due to a small pore volume of the composite (0.29 $cm^2 g^{-1}$).

A single and novel manganese-based metal-organic framework known as UPMOF-4 was solvothermally synthesized, with 1,2,4-triazole and N, N′-dimethylacetamide as the ligand and solvent, respectively. The UPMOF-4 demonstrated a specific capacity as high as 203.1 $C g^{-1}$ in 1 M potassium hydroxide. The UPMOF-4 showed a battery-type characteristic, verified by Dunn's method, in which the *b* value is 0.502, and distinct redox peaks and plateaus were observed in the cyclic voltammetry and galvanostatic charge–discharge curves, respectively. As a device, the UPMOF-4//activated carbon displayed a superior

specific energy of 32.97 Wh kg^{-1} and a specific power of 543 W kg^{-1}. As a result of the presence of an abundant porous structure and remarkable structural stability, the UPMOF-4 possesses excellent cycling stability and 78.2% capacity retention for 10,000 cycles [5]. Another novel single manganese-based MOF identified as UPMOF-5, was synthesized by Raman et al. [6]. The unique morphology, which was uniformly stacked, provided a large surface area of 1724 m^2 g^{-1} with a pore diameter and pore volume of 1.10 nm and 0.573 cm^2 g^{-1}, respectively. In a three-electrode system in which the electrolyte used was 1 M potassium hydroxide, the UPMOF-5 established a specific capacity of 160.17 C g^{-1}. As a device, the UPMOF-5//activated carbon exhibits specific capacity, specific energy, and a specific power of 132.40 C g^{-1}, 24.77 Wh kg^{-1}, and 538.91 W kg^{-1}. In addition, the device exhibits 70.3% capacitance retention after 10,000 cycles.

In this work, a copper-based metal-organic framework, identified as the HKUST-1, was prepared via a facile hydrothermal method. The HKUST-1 was introduced as a positive electrode for supercapattery due to the positive traits of the HKUST-1, such as its large specific surface area and the presence of abundant mesopores, which are beneficial in charge storage and allow for the easy transportation of charges between the electrolyte and electrode region. In order to further evaluate the real application of the HKUST-1, the battery-type HKUST-1 was assembled with N-doped graphene, a capacitive-type negative electrode. The integration of the HKUST-1 and N-doped graphene in a single device synergistically enhances the device's electrochemical performance. This is attributable to the good redox activity of the HKUST-1, as well as its large specific surface area, complemented by the good mechanical strength and high conductivity of the N-doped graphene. Thus, the HKUST-1 is a highly promising candidate for the positive electrode for the next generation of high-performance supercapattery devices.

2. Materials and Methods

2.1. Materials

Carbon mesoporous, polytetrafluoroethylene (PTFE), and trimesic acid were obtained from Sigma Aldrich (St. Louis, MA, USA). Acetone (99.5%) and hydrochloric acid (HCl) (95%) were acquired from Bendosen (Holtålen, Norway) and R&M Chemicals (Chandigarh, India), respectively. Ethanol (95%), lithium hydroxide (LiOH), and copper nitrate trihydrate Cu(NO$_3$)$_2$·3H$_2$O were obtained from HmbG (Denton, TX, USA) and Merck KgaA (Darmstadt, Germany), respectively. Nickel foam was purchased from Goodfellow (San Angelo, TX, USA), whereas graphene oxide was obtained from Graphenea SA (Boston, MA, USA). Throughout the experiment, a Millipore system of deionized water (18.2 MΩ.cm) was used for the preparation of the solution.

2.2. Synthesis of the HKUST-1

Trimesic acid (0.42 g) was dissolved completely in ethanol (12 mL), and copper nitrate Cu(NO$_3$)$_2$ (0.875 g) was fully dissolved in deionized water (12 mL). The Cu(NO$_3$)$_2$ solution was then added into the trimesic acid solution and stirred for 1 hour before being subjected to hydrothermal. The hydrothermal was carried out at 120 °C for 16 h, followed by the drying of the HKUST-1 in the oven at 90 °C for 2 h.

2.3. Synthesis of N-Doped Graphene

An aqueous solution of graphene oxide (1 mg mL^{-1}) was prepared and sonicated for 30 min to exfoliate the graphene layers. A total of 20 mg mL^{-1} of urea, which acts as a nitrogen source, was added into the graphene oxide solution and stirred for another 30 min. The mixture was sealed in a stainless-steel autoclave and subjected to a hydrothermal process for 12 h at 180 °C. The product that was in a hydrogel form was then filtered and washed a few times using deionized water to remove impurities and unreacted chemicals. The hydrogel was then freeze-dried in order to maintain the structure of the N-doped graphene.

2.4. Characterization

A field-emission scanning electron microscope (FESEM) (JEOL JSM 7600F, Pleasanton, CA, USA) was utilized to observe the surface morphology of the HKUST-1. The structural fingerprint of the HKUST-1 was analyzed using a Raman spectrometer (WITec GmbH, Ulm, Germany) with a 532 nm excitation laser. In order to determine the functional groups of the samples, Fourier-transform infrared spectroscopy (FTIR) (Shimadzu, Kyoto, Japan) was conducted in a wavelength range of 4000–500 cm^{-1}. The phase identification and crystallography of the sample were studied in the scanning range of 5–60° using an X-ray diffractometer (XRD) (Shimadzu 6000, Kyoto, Japan) with Cu Kα as the X-ray source (λ = 1.54 Å). The surface area, pore volume, and pore diameter of the HKUST-1 were investigated from the N$_2$ adsorption–desorption isotherm (MicroActive for Tristar II, Micromeritics, GA, USA).

2.5. Electrochemical Analyses

The electrochemical analyses were investigated in 1 M LiOH using an electrochemical analyzer (PGSTAT204, Metrohm Autolab, Utrecht, THE Netherlands) utilizing the HKUST-1 on nickel foam as a working electrode, platinum (Pt) wire as a counter electrode, and Ag/AgCl as a reference electrode. The nickel foam (1 cm^2) was subsequently washed with acetone, HCl, and deionized water before drying overnight at 60 °C. The working electrode was fabricated by forming a homogenous slurry mixture of 80% active materials, 10% carbon mesoporous, and 10% PTFE in ethanol coated on the nickel foam. The mass loading of the active material was 28 mg/cm^2. The cyclic voltammetry was performed at various scan rates from 0 to 0.6 V. The specific capacity, C_s (C g^{-1}), was determined from cyclic voltammetry curves using Equation (1) [2]:

$$C_s = \frac{\int I dV}{vm} \tag{1}$$

where v (V s^{-1}) is the scan rate, m (g) is the mass of active materials, and $\int_{V_i}^{V_f} IV dv$ is the area of the CV curve.

Galvanostatic charge–discharge was carried out at different current densities (1 to 5 A/g) at the same potential window as cyclic voltammetry (0 to 0.6 V). From the galvanostatic charge–discharge curves, C_s was calculated using Equation (2) [7]:

$$C_s = \frac{I \Delta t}{m} \tag{2}$$

where I is current (A), Δt is discharging time (s), and m is the mass of the active materials (g).

In order to study the resistivity of the HKUST-1, electrochemical impedance spectroscopy was performed from 0.1 Hz to 100 kHz with an AC amplitude of 5 mV at an open circuit potential.

2.6. Supercapattery Assembly and Electrochemical Measurement

The electrochemical measurement of the supercapattery device of the HKUST-//N-doped graphene (HKUST-1//NDG) was performed using a potentiostat. A gel polymer electrolyte, PVA-LiOH, was used as the electrolyte for the HKUST-1//NDG. This gel polymer electrolyte was prepared by dissolving 1 g PVA in 10 mL of deionized water and agitated at 80 °C until the solution turned clear. Then, 1 g of LiOH was added to the clear solution, and stirring continued for a few hours. In order to fabricate the device, a filter paper soaked in PVA/LiOH was sandwiched between the HKUST-1 and N-doped graphene. The specific energy (*E*) and specific power (*P*) of the HKUST-1//NDG were obtained from the galvanostatic charge–discharge curves using Equation (3) [8] and Equation (4) [8], respectively:

$$E = \frac{C_s \times \Delta V}{2 \times 3.6} \tag{3}$$

$$P = \frac{E \times 3600}{\Delta t} \tag{4}$$

where Δt is discharging time (s) and ΔV is the potential window (V).

3. Results and Discussion

3.1. Physicochemical Characterizations

The surface morphology of the HKUST-1 is shown in Figure 1a. The HKUST-1 displays a typical octahedral structure. The N_2 adsorption–desorption isotherm of the HKUST-1 (1b) illustrates type IV with a hysteresis loop (P/P_o = 0.5 to 1.0), indicating the presence of mesopores in the material, which is consistent with the average pore size (2.64 nm) calculated using the Barrett–Joyner–Halenda (BJH) method [9]. The HKUST-1 exhibits a BET-specific surface area of 1015.02 m^2 g^{-1} with a specific pore volume of 0.53 cm^{-1} g^{-1}, which indicates that the HKUST-1 offers an abundance of pores with a large specific surface area, which is beneficial for maximizing the electrochemical reaction.
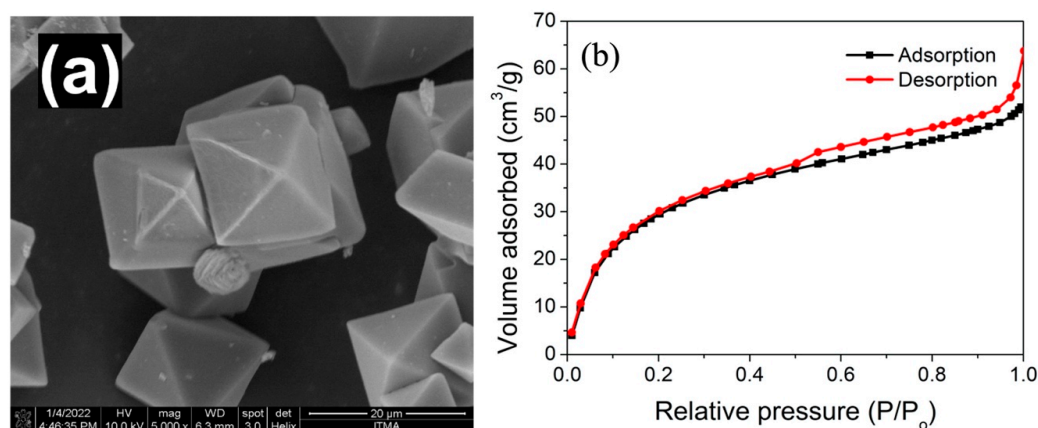

Figure 1. (**a**) FESEM image of the HKUST-1 and (**b**) the N_2 adsorption–desorption isotherm of the HKUST-1.

The Raman spectrum (Figure 2a) shows a peak of Cu-Cu at 190 cm^{-1} and a peak at 290 cm^{-1} due to the O-Cu-O bond stretching vibration modes, whereas the Cu-O stretching vibration bonds that predominantly indicate the carboxylate bridges can be observed at 500 cm^{-1}. The peaks observed at 730 and 815 cm^{-1} indicate the carbonyl group (CO) and C-H bending vibration modes, respectively. The stretching mode of C=C of benzene can be observed at 1000 cm^{-1}, and the bond of vibration mode and linked stretching for the carboxylate group are related to both peaks at 1465 cm^{-1} and 1535 cm^{-1}, respectively [10]. Figure 2b shows the FTIR spectrum of the HKUST-1, which displays a broad peak that is centralized at 3300 cm^{-1} and manifests the presence of hydroxyl groups. The CO-OH bond and C-OH bond are determined at 1625 cm^{-1} and 1125 cm^{-1}, respectively. The carboxyl group is found at 1460 cm^{-1} and 1375 cm^{-1} for both symmetric and asymmetric stretching vibration, respectively. The bending and stretching of Cu-O is noticed at 745 cm^{-1} [11]. The crystallinity and the chemical phase of the HKUST-1 were determined via XRD. The diffraction peaks (Figure 2c) are observed at 7.1°, 9.5°, 11.7°, 13.4°, 14.7°, 17.6°, 19.1°, 19.9°, 20.9°, 23.2°, 23.7°, 26.0°, 27.6°, 28.5°, and 29.7° [12], indicating that the HKUST-1 has a microporous crystal framework [12]. The presence of sharp and obvious peaks below 20° indicates the successful formation of the HKUST-1, while the remaining peak can be allocated to Cu_2O (JCPDS: 5-0667) and CuO (JCPDS: 45-0937). The XRD pattern of the HKUST-1 is consistent with the XRD pattern of the simulated HKUST-1, proving that the pure HKUST-1 is formed [12,13].
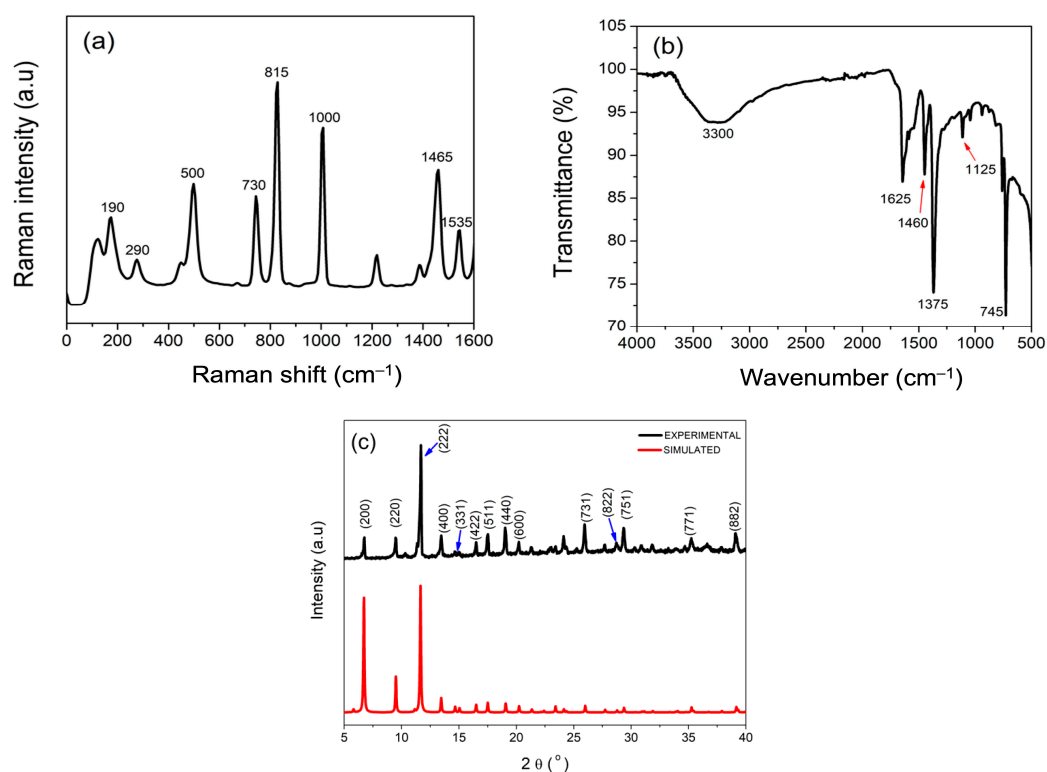
Figure 2. (**a**) Raman spectrum, (**b**) Fourier-transform infrared spectrum, and (**c**) X-ray diffraction pattern of the HKUST-1.

3.2. Electrochemical Characterization

The cyclic voltammetry of the HKUST-1 was performed in a three-electrode system at a potential window of 0–0.6 V at various scan rates, with 1 M LiOH as the electrolyte. Figure 3a depicts the cyclic voltammetry curves of the HKUST-1 with obvious pairs (0.45 and 0.25 V) of redox peaks at all scan rates due to the redox Faradaic reaction, verifying its battery-type property [14]. The cyclic voltammetry curves maintain their battery-type shape and the peak current increases as the scan rate increases, indicating the rapid rate of the mobile ion transports in the HKUST-1 [15]. The specific capacity of the HKUST-1 was calculated using Equation (1). The specific capacity of the HKUST-1 electrode at 1 mV s^{-1} is 126.2 C g^{-1}; whereas, at 5 mV s^{-1}, the specific capacity of the HKUST-1 is 62.7 C g^{-1}. Figure 3b shows the plot of the specific capacity of the HKUST-1 at different scan rates. The specific capacity gradually decreases as the scan rates increase due to the slow diffusion process of ions accessing the inner surface electrode at high scan rates [16].

The mechanism of charge storage of the HKUST-1 was studied to confirm whether it is a diffusion-controlled or a non-diffusive process by analyzing the cyclic voltammetry curves at different scan rates using Equation (5), which is known as Power's law [17]:

$$i = a v^b \tag{5}$$

where i is the cathodic current peak (A) and ν is the scan rate (V s^{-1}), whereas a and b are variable parameters. The b value can determine the charge-storing mechanism of the HKUST-1. Therefore, the graph of the log cathodic peak current vs. the log scan rate was plotted in Figure 3c to obtain the b value. The obtained b value (0.52) is near 0.5, implying that the HKUST-1 possesses a diffusion-controlled charge storage mechanism and confirming the battery-type property of the HKUST-1 [18,19].
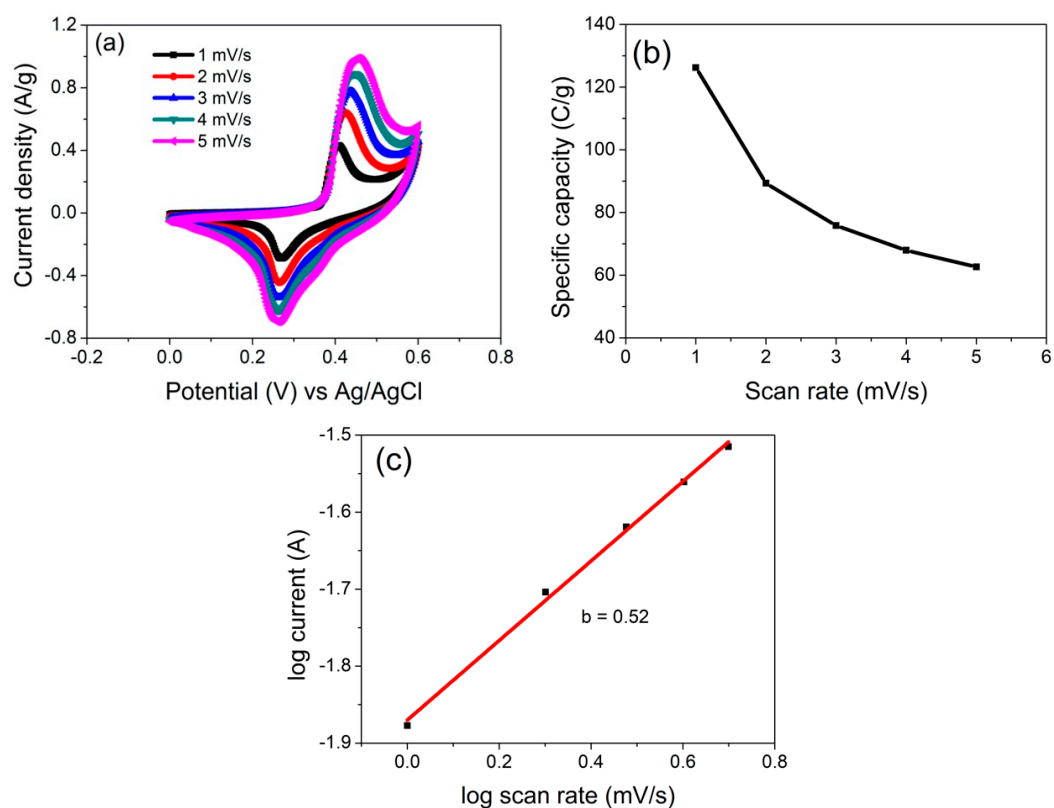
Figure 3. (**a**) Cyclic voltammetry curves of the HKUST-1 at different scan rates in 1 M LiOH, (**b**) specific capacity vs. scan rate, and (**c**) log peak current against log scan rate.

The electrochemical performance of the HKUST-1 was further analyzed by galvanostatic charge–discharge via a three-electrode system in 1 M LiOH. The measurement was carried out at current densities between 1 and 5 A g^{-1} within 0–0.6 V. The charge–discharge curves of the HKUST-1 (Figure 4a) display a plateau at 0.2 V, showing a Faradaic redox reaction occurring in the system, which indicates that the HKUST-1 is a battery-type material [20]. The discharging time increases at low current densities as the ions in the electrolyte obtain sufficient time to interact with the electrode's material [21]. The specific capacity of the HKUST-1 was calculated for each current density in Equation (2), and the maximum specific capacity obtained is 15.7 C g^{-1} as a result of the large surface area together with the high pores volume of the HKUST-1.
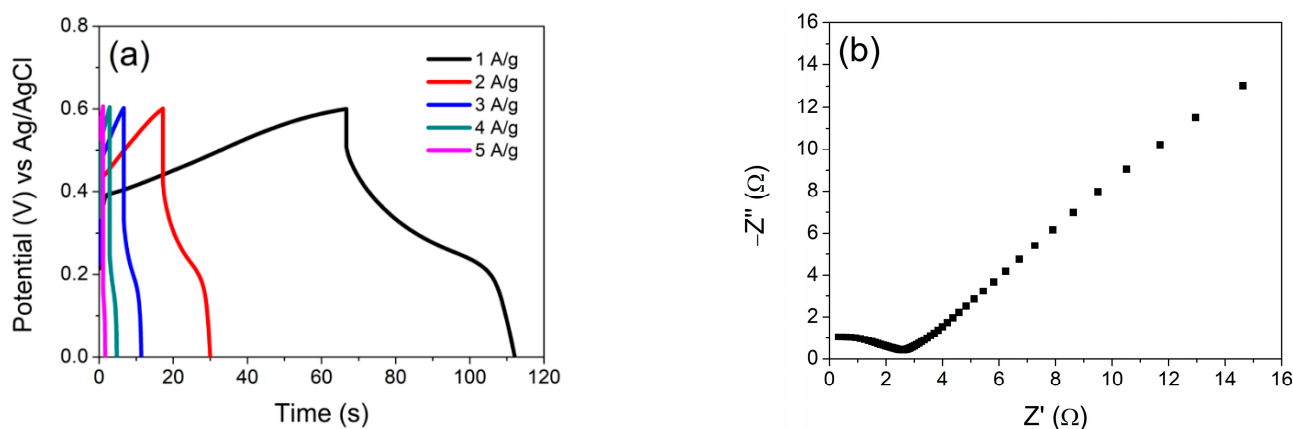

Figure 4. (**a**) Galvanostatic charge–discharge curves of the HKUST-1 at various current densities (1–5 A/g) and (**b**) Nyquist plots of the HKUST-1 in 1 M LiOH.

Electrochemical impedance spectroscopy measurement of the HKUST-1 was also performed in a three-electrode system in 1 M LiOH to further determine the resistivity of the HKUST-1. At the high-frequency region of the Nyquist plot (Figure 4b), the diameter of the semicircle indicates the interfacial charge transfer resistance between the HKUST-1 electrode's surface and electrolyte ions [22], whereas the intersection on the *x*-axis refers to the equivalent series resistance, which includes the intrinsic resistance of the HKUST-1, interfacial resistance between 1 M LiOH and the HKUST-1, and resistance between nickel foam and the HKUST-1. On the other hand, at the lower frequency region, Warburg impedance (W) can be demonstrated from the straight line [23]. The equivalent series resistance value for the HKUST-1 is 0.08 Ω, while the charge transfer resistance value for the HKUST-1 is 2.62 Ω. These indicate that the HKUST-1 exhibits high conductivity and low charge transfer resistance [15].

3.3. Electrochemical Performance of Assembled Supercapattery

Figure 5a shows the cyclic voltammetry curves of the HKUST-1 and N-doped graphene in a three-electrode configuration at 1 mV/s in 1 M LiOH. The operating potential window for the battery-type HKUST-1 is 0–0.6 V, whereas the operating window for the capacitive N-doped graphene is −0.6–0 V, which suggests that the supercapattery device can be operated between 0 and 1.2 V [24]. The cyclic voltammetry analysis of the HKUST-1//N-doped graphene at different scan rates from 0 to 1.2 V was carried out using PVA/LiOH gel as an electrolyte. The cyclic voltammetry curves (Figure 5b) illustrate both contributions from capacitive and battery-type behavior at all scan rates, which are confirmed by the calculated b-value (0.41) of the HKUST-1//N-doped graphene. In addition, the shape of the cyclic voltammetry curves is maintained, even at high scan rates, indicating its good rate capability. Galvanostatic charge–discharge analysis of the HKUST-1//N-doped graphene was also carried out from 0 to 1.2 V at various current densities, as shown in Figure 5c. The curves reveal a plateau observed at ~1.0 V during the discharging curve, indicating that the HKUST-1 possesses a battery-type charge storage mechanism, whereas a linear curve is observed during the charging curve between 0.8 and 0.2 V, implying the capacitive nature of the N-doped graphene [25]. The specific energy and the specific power of the HKUST-1//N-doped graphene were calculated using Equations (3) and (4), respectively. The specific energy and specific power of the device are 2.61 Wh kg^{-1} and 600 W kg^{-1} at 1 A g^{-1}. Figure 5d illustrates the Ragone plot of the HKUST-1//N-doped graphene, which shows that the specific power increases as the specific energy decreases.

The resistivity of the HKUST-1//N-doped graphene was studied via electrochemical impedance spectroscopy at an open circuit potential with a frequency of 0.1–100 kHz (amplitude, 5 mV). The Nyquist plot (Figure 5e) shows a semicircle at the high-frequency region, and the charge transfer resistance and equivalent series resistance values for the device are 7.86 Ω and 0.87 Ω, respectively. These values indicate that the device has excellent conductivity and exhibits low equivalent series resistance, which is due to the large surface area and mesoporous structure of the HKUST-1 that provides efficient transportation of electrolyte ions. The equivalent circuit of the HKUST-1//NDG is displayed in the inset Figure 5e. The equivalent circuit consists of ESR, R_{ct}, constant phase elements (CPEs), and Warburg (W) elements. Furthermore, the cycle stability of the device was analyzed by galvanostatic charge–discharge measurements at 0.2 A g^{-1} for 10,000 cycles, as depicted in Figure 5f. It can be observed that the capacity retention decreases are attributable to the low structural stability of the HKUST-1 after repeated charging–discharging cycles. It is well known that metal-organic framework has low structural stability due to the collapsing of its framework after repeated and continuous charging–discharging cycles. However, with the presence of the high mechanical stability of N-doped graphene, the device is able to retain 57% after continuous 10,000 charging–discharging cycles. The device exhibits decent cycling retention on account of the synergistic effect between both the HKUST-1 and the N-doped graphene [26].
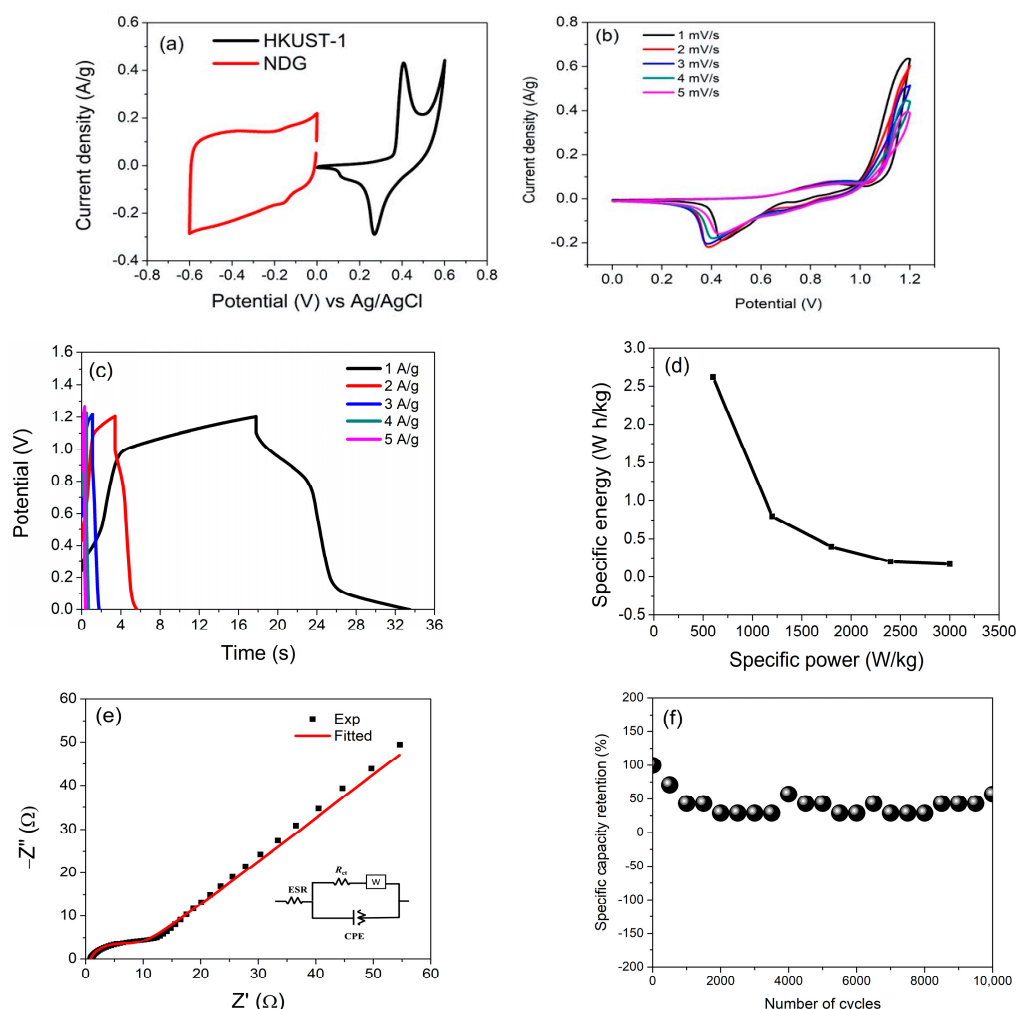
Figure 5. (**a**) Cyclic voltammetry curve of the HKUST-1 and N-doped graphene, respectively, at 1 mV/s via three-electrode configuration in 1 M LiOH, (**b**) cyclic voltammetry curves of the HKUST-1//N-doped graphene measured at diverse scan rates, (**c**) galvanostatic charge–discharge curves of the HKUST-1//N-doped graphene assessed at various current densities, (**d**) Ragone plot of the HKUST-1//N-doped graphene, (**f**) Nyquist plot of the HKUST-1//N-doped graphene (inset: equivalent circuit of the HKUST-1//NDG), and (**e**) cycling stability of the HKUST-1//N-doped graphene supercapattery for 10,000 cycles.

4. Conclusions

A battery-type copper-based metal-organic framework, the HKUST-1, was prepared via the hydrothermal method, and its electrochemical performance for a supercapattery in 1 M LiOH was successfully evaluated. The prepared HKUST-1 displayed an octahedral structure with a large specific surface area and pore volume. The HKUST-1 also showed high crystallinity and diffraction peaks, which were similar to the simulated HKUST-1. The HKUST-1 demonstrated a specific capacity of 15.7 C g^{-1}, as well as good conductivity, due to the high pore volumes (0.53 cm^{-1} g^{-1}) and large specific surface area (1015.02 m^2 g^{-1}) of the HKUST-1. A supercapattery device with a total potential window of 1.2 V consisting of the HKUST-1 was a positive electrode, and N-doped graphene was a negative electrode; they exhibited 2.61 Wh kg^{-1} and 300 W kg^{-1} of specific energy and specific power, respectively, at 1 A/g, with a capacity retention of 57% after 10,000 cycles. These significant findings indicated that the HKUST-1 displayed a promising positive electrode material for supercapattery devices.

References

1. Faisal, M.M.; Ali, S.R.; Sanal, K.C.; Iqbal, M.W.; Iqbal, M.Z.; Saeed, A. Highly porous terpolymer-MOF composite electrode material for high performance supercapattery devices. *J. Electroanal. Chem.* **2021**, *893*, 115321. [CrossRef]
2. Iqbal, M.Z.; Faisal, M.M.; Ali, S.R.; Alzaid, M. A facile approach to investigate the charge storage mechanism of MOF/PANI based supercapattery devices. *Solid State Ion.* **2020**, *354*, 115411. [CrossRef]
3. Raihana, M.K.; Padmanathan, N.; Eswaramoorthi, V.; McNulty, D.; Sahadevan, J.; Mohanapriya, P.; Muthu, S.E. Reduced graphene oxide/VSB-5 composite micro/nanorod electrode for high energy density supercapattery. *Electrochim. Acta* **2021**, *391*, 138903. [CrossRef]
4. Ramasubbu, V.; Omar, F.S.; Ramesh, K.; Ramesh, S.; Shajan, X.S. Three-dimensional hierarchical nanostructured porous TiO_2 aerogel/Cobalt based metal-organic framework (MOF) composite as an electrode material for supercapattery. *J. Energy Storage* **2020**, *32*, 101750. [CrossRef]
5. Raman, V.; Gándara, F.; Azman, N.H.N.; Mohamed Tahir, M.I.; Abdul Rahman, M.B.; Sulaiman, Y. Facile synthesis and characterisations of novel Mn-1,2,4-triazole framework (UPMOF-4) as a promising electrode material for supercapattery device. *J. Energy Storage* **2023**, *62*, 106867. [CrossRef]
6. Raman, V.; Gándara, F.; Mohamed Tahir, M.I.; Abdul Rahman, M.B.; Sulaiman, Y. 1,2,4-Triazole (Htrz) functionalised 2D-manganese-organic framework (UPMOF-5) as a battery-type electrode for supercapattery. *J. Electroanal. Chem.* **2023**, *929*, 117122. [CrossRef]
7. Iqbal, J.; Numan, A.; Ansari, M.O.; Jagadish, P.R.; Jafer, R.; Bashir, S.; Mohamad, S.; Ramesh, K.; Ramesh, S. Facile synthesis of ternary nanocomposite of polypyrrole incorporated with cobalt oxide and silver nanoparticles for high performance supercapattery. *Electrochim. Acta* **2020**, *348*, 136313. [CrossRef]
8. Iqbal, J.; Numan, A.; Jafer, R.; Bashir, S.; Jilani, A.; Mohammad, S.; Khalid, M.; Ramesh, K.; Ramesh, S. Ternary nanocomposite of cobalt oxide nanograins and silver nanoparticles grown on reduced graphene oxide conducting platform for high-performance supercapattery electrode material. *J. Alloys Compd.* **2020**, *821*, 153452. [CrossRef]
9. Ediati, R.; Laharto, P.B.F.; Safitri, R.; Mahfudhah, H.; Oktavia Sulistiono, D.; Denisa Syukrie, T.; Nadjib, M. Synthesis of HKUST-1 with addition of Al-MCM-41 as adsorbent for removal of methylene blue from aqueous solution. *Mater. Today Proc.* **2021**, *46*, 1799–1806. [CrossRef]
10. Amrollahi Bioki, H.; Moshaii, A.; Borhani Zarandi, M. Performance improvement of ambient-condition fabricated perovskite solar cells using an interfacial HKUST-1 MOF on electron transfer layer. *Surf. Interfaces* **2021**, *27*, 101579. [CrossRef]
11. Ai, Y.; Gao, N.; Wang, Q.; Gao, F.; Hibbert, D.B.; Zhao, C. Electrosynthesis of HKUST-1 on a carbon-nanotube-modified electrode and its application for detection of dihydroxybenzene isomers. *J. Electroanal. Chem.* **2020**, *872*, 114161. [CrossRef]
12. Zhao, H.; Lei, M.; Liu, T.; Huang, T.; Zhang, M. Synthesis of composite material HKUST-1/LiCl with high water uptake for water extraction from atmospheric air. *Inorg. Chim. Acta* **2020**, *511*, 119842. [CrossRef]
13. Dong, J.; Li, P.; Guan, H.; Ge, C.; Bai, Y.; Zhao, Y.; Zhang, X. The synthesis of $HKUST-1/SiO_2$ composite material based on 3D printing. *Inorg. Chem. Commun.* **2020**, *117*, 107975. [CrossRef]
14. Iqbal, M.Z.; Khan, J.; Gul, A.; Siddique, S.; Alzaid, M.; Saleem, M.; Iqbal, M.J. Copper doped cobalt-manganese phosphate ternary composites for high-performance supercapattery devices. *J. Energy Storage* **2021**, *35*, 102307. [CrossRef]
15. Kim, B.C.; Manikandan, R.; Yu, K.H.; Park, M.-S.; Kim, D.-W.; Park, S.Y.; Justin Raj, C. Efficient supercapattery behavior of mesoporous hydrous and anhydrous cobalt molybdate nanostructures. *J. Alloys Compd.* **2019**, *789*, 256–265. [CrossRef]
16. Shahabuddin, S.; Numan, A.; Shahid, M.M.; Khanam, R.; Saidur, R.; Pandey, A.K.; Ramesh, S. Polyaniline-$SrTiO_3$ nanocube based binary nanocomposite as highly stable electrode material for high performance supercapaterry. *Ceram. Int.* **2019**, *45*, 11428–11437. [CrossRef]
17. Iqbal, M.Z.; Alam, S.; Afzal, A.M.; Iqbal, M.J.; Yaqoob, K.; Kamran, M.A.; Karim, M.R.A.; Alherbi, T. Binary composites of strontium oxide/polyaniline for high performance supercapattery devices. *Solid State Ion.* **2020**, *347*, 115276. [CrossRef]
18. Iqbal, M.Z.; Faisal, M.M.; Sulman, M.; Ali, S.R.; Alzaid, M. Facile synthesis of strontium oxide/polyaniline/graphene composite for the high-performance supercapattery devices. *J. Electroanal. Chem.* **2020**, *879*, 114812. [CrossRef]
19. Iqbal, M.Z.; Khan, J. Optimization of cobalt-manganese binary sulfide for high performance supercapattery devices. *Electrochim. Acta* **2021**, *368*, 137529. [CrossRef]

20. Shinde, N.M.; Xia, Q.X.; Yun, J.M.; Shinde, P.V.; Shaikh, S.M.; Sahoo, R.K.; Mathur, S.; Mane, R.S.; Kim, K.H. Ultra-rapid chemical synthesis of mesoporous Bi_2O_3 micro-sponge-balls for supercapattery applications. *Electrochim. Acta* **2019**, *296*, 308–316. [CrossRef]

21. Haider, S.S.; Iqbal, M.Z.; Zakar, S.; Afzal, A.M.; Yaqoob, K.; Aftab, S. Superior performance of electrodeposited CoMnS as novel electrode material for supercapattery devices. *J. Energy Storage* **2021**, *39*, 102608. [CrossRef]

22. Oyedotun, K.O.; Madito, M.J.; Momodu, D.Y.; Mirghni, A.A.; Masikhwa, T.M.; Manyala, N. Synthesis of ternary NiCo-MnO_2 nanocomposite and its application as a novel high energy supercapattery device. *Chem. Eng. J.* **2018**, *335*, 416–433. [CrossRef]

23. Ramulu, B.; Chandra Sekhar, S.; Nagaraju, G.; Yu, J.S. Rational design and construction of nickel molybdate nanohybrid composite for high-performance supercapattery. *Appl. Surf. Sci.* **2020**, *515*, 146023. [CrossRef]

24. Gurusamy, L.; Karuppasamy, L.; Anandan, S.; Liu, N.; Lee, G.-J.; Liu, C.-H.; Wu, J.J. Enhanced performance of charge storage supercapattery by dominant oxygen deficiency in crystal defects of 2-D MoO_{3-x} nanoplates. *Appl. Surf. Sci.* **2021**, *541*, 148676. [CrossRef]

25. Alam, S.; Iqbal, M.Z. Nickel-manganese phosphate: An efficient battery-grade electrode for supercapattery devices. *Ceram. Int.* **2021**, *47*, 11220–11230. [CrossRef]

26. Tarimo, D.J.; Oyedotun, K.O.; Mirghni, A.A.; Mutuma, B.; Sylla, N.F.; Murovhi, P.; Manyala, N. Enhanced electrochemical performance of supercapattery derived from sulphur-reduced graphene oxide/cobalt oxide composite and activated carbon from peanut shells. *Int. J. Hydrogen Energy* **2020**, *45*, 33059–33075. [CrossRef]